Vacuum 86 (2012) 1828–1833

Contents lists available at SciVerse ScienceDirect

Vacuum

journal homepage: www.elsevier.com/locate/vacuum

Fracture responses of microstructures of electron beam-welded D6AC

Shyh-Chi Wu [a,b], Hua-Chiang Wen [a,c,*], Ming-Jhang Wu [a], Chang-Pin Chou [a]

[a] Department of Mechanical Engineering, National Chiao Tung University, Hsinchu 300, Taiwan, ROC
[b] Chung Shan Institute of Science and Technology (CSIST), Taoyuan 325, Taiwan, ROC
[c] Department of Materials Science and Engineering, National Tsing-Hua University, HsinChu 30013, Taiwan, ROC

ARTICLE INFO

Article history:
Received 22 December 2011
Received in revised form
26 March 2012
Accepted 26 March 2012

Keywords:
EBW
Tensile strength
Tempering
SEM

ABSTRACT

In this study, D6AC steel was produced from flow forming (wall thickness reduction: 67%) and then it was subjected to electron beam welding and tempering treated. We characterized the specimens in terms of their microstructures and nanotribological properties. After tempering treatment at 315 °C, the yield strength increased from 381 to 1334 MPa and the percentage elongation increased remarkably from 0.5 to 7.8%. We performed these mechanical studies for the samples subjected to each set of experimental conditions, and determined the tribological characteristics from the heat-affected zone and the fusion zone. Lower degrees of adhesion reflected the presence of interlinks and rearrangements of indenter tip at lateral force that have been responsible for fluctuations in the coefficients of friction.

1. Introduction

D6AC is a low-alloy vacuum-melted steel containing several other elements and featuring a carbon content of 0.42–0.48%. The hardenability of D6AC is better than that of AISI 4340, which can be heat-treated to strengths ranging from 1241 to 1793 ksi [1]. D6AC, a high strength steel, has been widely applied, for example, aircrafts and rocket cases because it provides a high tensile strength, good ductility, and good notch toughness at room temperature [1–3]. The flow forming method is a common metal forming process in the production of, for example, cylinders, flanged components, and axisymmetric sheet metal parts. Through the shear spinning of cones and tubes, the cold plastic forming technique can be used to form products exhibiting enhanced mechanical properties [4]. This approach has the attractive qualities of saving materials, allowing rapid processing, and cost effectiveness. After flow forming, electron beam welding (EBW) can be employed to weld the steel materials in a high-vacuum environment. The advantageous features of EBW include a low heat input to the metal being welded, a lack of oxidation on the surface of the work piece, a minimum amount of post-welding distortion, and a narrow heat-affected zone (HAZ) [5]. D6AC undergoes machining much like any of the other low-alloy steels. Machining is best done with the alloy in the normalized and tempered condition. Machining, or grinding, of parts that have been heat-treated to 200 ksi, or greater, require a 3-h stress relief anneal after such machining. Typically, massive residual stress remains and the formation of fibrous grains occurs after cold flow forming and post-welding. Post-weld aging is usually applied to eliminate these problems as well as the inadequate strength of the electron beam-welded material. High-temperature homogenization treatment of EBW metal specimens, however, can have detrimental effects on their mechanical properties. A suitable post-weld aging (tempering) treatment process can be used to overcome these problems. To test the mechanical properties of D6AC steel, nanoscratch technology can be applied for direct processing of the material's surfaces using a nano-sized tip; this analytical approach has several advantages, including the free selection of materials, simple design alteration, and convenient initial facilities [6]. EBW is a mature technology for creating high-quality welds on a work piece [7–9]. The low heat input of such a process results in the formation of narrow HAZs as well as fusion zones (FZs). Welding quality is usually affected by the HAZs; therefore, we focus the relation of fracture properties and nanotribological investigation of the EBW D6AC.

In this paper, we report the effects of tempering on EBW D6AC steel and the nanotribological properties of its HAZs and FZs. Our main goal for this study was to determine the nanotribological properties of the welded D6AC steel. We also performed a variance analysis of EBW D6AC steel to evaluate the effects of tempering treatment.

2. Experimental details

Chemical compositional analysis (Table 1) revealed that the contents of all the elements were within the ranges expected for

* Corresponding author. Room 412, ME-5 Building, 1001 Ta Hsueh Road, Hsinchu 300, Taiwan, ROC. Tel.: +886 3 5712121x55157; fax: +886 3 5733409.
E-mail address: a091316104@gmail.com (H.-C. Wen).

0042-207X/$ – see front matter © 2012 Elsevier Ltd. All rights reserved.
doi:10.1016/j.vacuum.2012.03.059

Table 1
Chemical composition of the D6AC steel (wt%).

Element	C	Mn	P	S	Si	Cr	Ni	Mo	V	Fe
Specification AMS 6431	0.42–0.48	0.6–0.9	0.01	0.01	0.15–0.3	0.9–1.2	0.4–0.7	0.9–1.1	0.08–0.15	Bal.
Used in this work	0.47–0.48	0.76–0.84	0.01	0.01	0.27	0.98–0.99	0.55	1.02–1.1	0.1	Bal.

standard D6AC (AMS 6431). The chemical composition of the steel was determined using energy dispersive X-ray spectrometry (EDS) and the carbon determination technique. The flow forming of D6AC steel plates was performed using the following procedure: (i) The D6AC steel was obtained through vacuum arc remelting (AMS 6431). (ii) Prior to the flow forming process, the D6AC steel was subjected to normalizing treatment (910 ± 14 °C), with a holding time of 105 min, and subsequent cooling in air. (iii) The flow forming of the D6AC steel was performed in a three-roller spinning machine (roller angles: 15, 20, and 30°) with the percentage reduction controlled at 67%. The specimens had thicknesses of 9.9 mm; the feed rate was 0.7 mm rpm^{-1}. (iv) The specimens are subjected to EBW in a vacuum welding chamber; the thermal input power during welding was 66.5 J mm^{-1} (detailed parameters are listed in Table 2). (v) The specimens were subjected to tempering treatment at 250 and 315 °C for 2 h, followed by air cooling.

Tensile test specimens were prepared following the guidelines of ASTM standard E370. These samples were separated by laser cutting along the axis direction of the tube, following ASTM standard E8a [10]. The morphologies of the tensile test specimens were characterized by scanning electron microscopy (SEM, Hitachi S-4300, Tokyo, Japan); the microstructures of the fracture surfaces are presented. Optical microscopy (OM) was used to characterize the morphologies of the regions after EBW. The nanotribological properties of the specimens were determined through nanoscratch tests performed using atomic force microscopy (AFM, Digital Instruments Nanoscope III) in conjunction with a nanoindentation measurement system (Hysitron); a constant scan speed of 2 μm s^{-1} was applied. To determine the fracture and abrasion of D6AC steel initiated at low-ramped-force modes of sliding cycles, specimens were subjected to ramped loads of 500 μN. With this approach, the corresponding surface profiles were obtained and 10-μm-long scratches were formed in the ramped-forces mode. The tip was applied to the samples at room temperature with loads ranging from 0 to 500 μN. The coefficient of friction (μ), defined as the ratio of the friction force (F) to the normal force (N) according to Amonton's law [11], is a useful parameter for estimating the nanotribological behavior of specimens; plots of μ with respect to the scratch duration were obtained.

3. Results and discussion

Fig. 1(a) displays a cast microstructure featuring dendrites with long branches following the heat flow during the rapid solidification process. Fig. 1(b) and (c) reveals that the grain boundaries of the solidified HAZ after tempering were clearer. In early literature, the Time–Temperature–Transformation diagram (TTT curve) of D6AC was noted to provide an Ms temperature of approximately 300 °C [12]. It was suggested that the Ms temperature would be lowered under the conditions required for the transformation of austenite into martensite. We suspected that tempering would help to eliminate the dislocations and the residual stress generated by the cold work [13–15].

Table 2
Parameters of EBW.

Accelerating voltage, kV	120
Beam current, mA	200
Vacuum level, Pa	1.32×10^{-2}
Gun to work distance (focal length), mm	444.5
Speed, mm min^{-1}	2100
Preheating	None
Post-heating	None
Pass number	1

The ductility behavior led to similarities in the plots of the hardness profiles of the HAZ and FZ (Fig. 2). The hardness profile of the FZ decreased from 63.2 to 44.2 H_{RC} upon increasing the treatment temperature from RT to T-315; the hardness profile of the HAZ also decreased upon increasing the temperature up to T-315 and then remained nearly constant at 36–40 H_{RC}. We attribute this behavior to the austenite phase transforming into martensite, which can decrease the hardness profile of the FZ and HAZ. Importantly, a much larger applied stress is needed to cause a dislocation slip to pass through the boundary in a fine-grained crystal than in a coarse-grained crystal at RT. The stable state of the hardness profile was found due to the austenite phase transforming into martensite and the residual austenite formation after tempering. Thus, the strength decreased upon increasing the temperature. We also examined the tempering effect through observations of the microstructures of the samples before and after EBW. We performed OM examinations of EB-welded section views that were generally consistent with the HAZ and FZ.

In order to investigate the trend of tempering, Table 3 lists the mechanical properties of the materials [yield strength (YS), ultimate tensile strength (UTS), and elongation]. Tempering treatment of the EBW sample resulted in the YS of the weldment (1334 MPa) exceeding the value of 1310 MPa stipulated in specification AMS6431M. However, the UTS of D6AC steel (1481 MPa) was less than the AMS6431M specification of 1517–1724 MPa, representing the softening values obtained through tempering in this study. Herein, tempering treatment can produce brittle precipitates for increased weldment strength of EBW D6AC steel. The average percentage elongations for the samples tempered at RT, 250 °C, and 315 °C were 0.5, 7.2, and 7.8%, respectively. Chang et al. [16] reported similar mechanical properties for their tempered D6AC samples, with the hardness and strength of the specimens decreasing upon increasing the tempering temperature. The YS of tempered steels can be affected by several mechanisms, such as substructure hardening and precipitate hardening. In our experimental results, the change in the microstructures of D6AC based on tempering is observed to eliminate dislocations and residual stress (Fig. 2). In addition, it is generally believed [17] that a high YS is associated with a material possessing an inherently low fracture toughness. Thus, we would expect a decrease in the plastic zone size during the tensile test upon increasing the YS of a sample. In Bannister et al. [18], they discussed the steel specifications for Y/T, YS, and UTS as specifically defined limits; current design code limits for Y/T vary between 0.70 and 0.90. There is strong agreement that values up to 0.85 are satisfactory in conventional structural applications, with values up to 0.95 being required in specific cases. We observe that the Y/T ratio here is increased from 0.855 to 0.901 at the increased temperatures. The average percentage elongations of the samples tempered from RT to 315 °C were all in the range from 0.5 to 7.8%. It is noted that limits to the Y/T ratio were considered in the design codes based

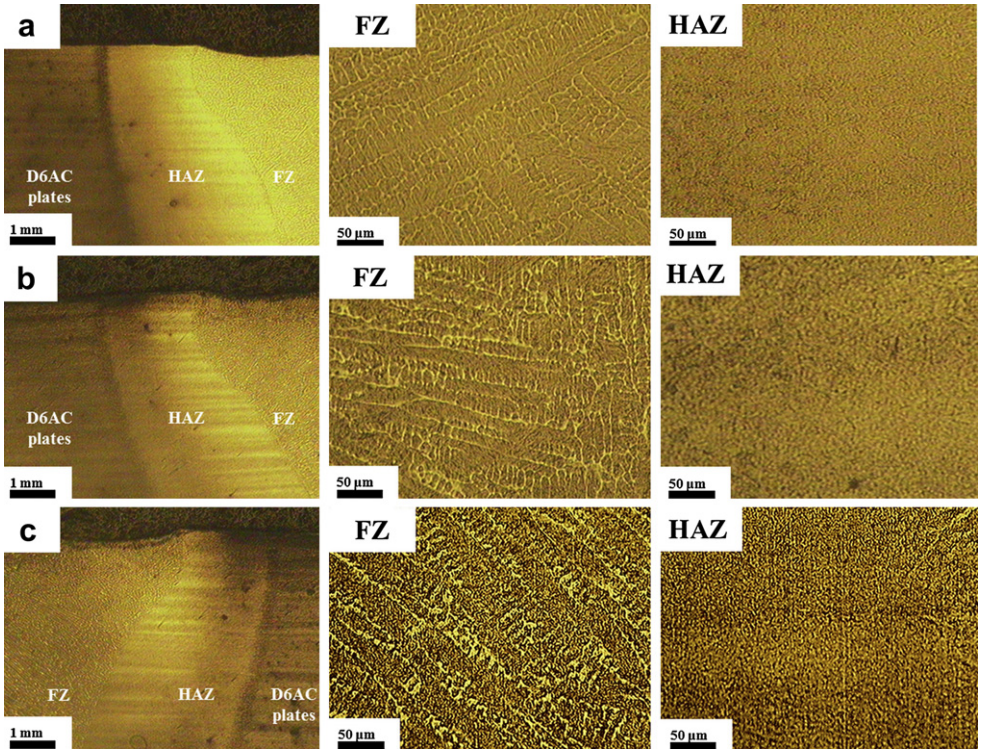

Fig. 1. OM images revealing the microstructures and macrostructures (insets are HAZ and FZ) of the tempering-hardened weld metal samples.

on the behavior of steels and the notion that a high Y/T value equates to poor fracture performance [19]. Next, we used SEM to view cross-sectional images of the D6AC steel after tensile testing.

Fig. 3(a) shows the microstructures of the fracture surfaces is rupture with large dimple at room temperature. In Fig. 3(b) and (c), the microstructures of the fracture surfaces present ductile rupture with small dimple. The similar fracture surfaces observed after tempering treatment at 250 and 315 °C suggest that high-density martensitic structures induce many dislocations as well as dislocation slips that may deform the material in slip bands under tensile stress. In order to investigates the role of dislocations, TEM is employed to analyze the microstructure of D6AC steel. Fig. 4 reveals

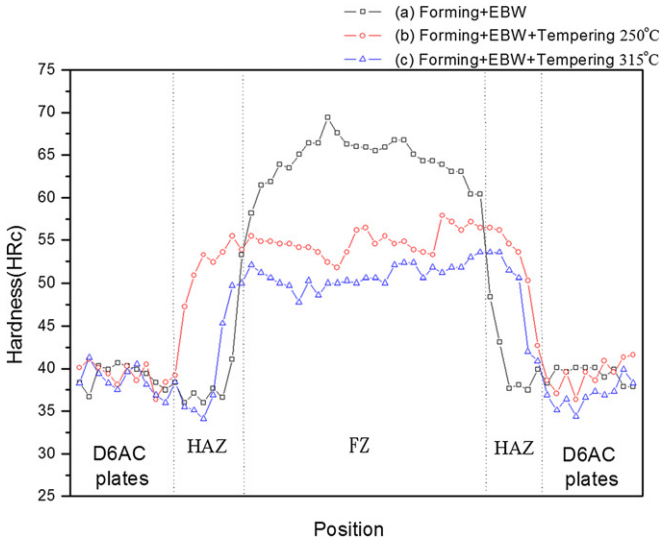

Fig. 2. Hardness profiles of the HAZ and FZ.

plane-view TEM image of original D6AC steel at RT. The heavily misfit dislocations by work hardening is displayed (Fig. 4(a)). We can observe dislocation multiplication or through dislocation nucleation that induces some extended grain shape. Contrary, the samples tempered after 250 °C, disorder dislocation is still produced else (Fig. 4(b)). We can observe few dislocation multiplication or through dislocation nucleation due to the thermally environment (Fig. 4(c)). The flow-formed D6AC is consisted of large dislocation nucleation from heavily cold worked, and therefore given an additional tempering treatment to avoid the immediately fracture impact. In addition, the degree of porosity of the fracture surfaces in the weld metal increased upon increasing the ferrite content. In general, the loss of work hardening of a material can occur after tempered of the weld metal. We found that direct tempering treatment yielded greater strength and elongation.

To compare the nanotribological behavior of the HAZs before and after tempering of the D6AC steel, we initiated the abrasion at HAZ and FZ than that of the parent material at ramped forces of the sliding cycles. Fig. 5 plots the fluctuations in lateral force with respect to the duration of displacement from (a) the parent material, (b) the HAZ, and (c) the FZ. The applied load increased over time. Fig. 5(a) reveals the less fluctuations of the lateral force over the entire surface of the parent material. The specimens tempered

Table 3
Mechanical properties of flow-formed D6AC steel materials subjected to tempering heat treatment.

D6AC sample code	Heat treating process	YS (0.2% offset), MPa	UTS, MPa	Y/T ratio	Elongation (gauge 50.8 mm), %
RT	Solution + forming + EBW	380	608	0.625	0.5
250 °C	Solution + forming + EBW + heat treatment	1263	1477	0.855	7.2
315 °C	Solution + forming + EBW + heat treatment	1334	1481	0.901	7.8

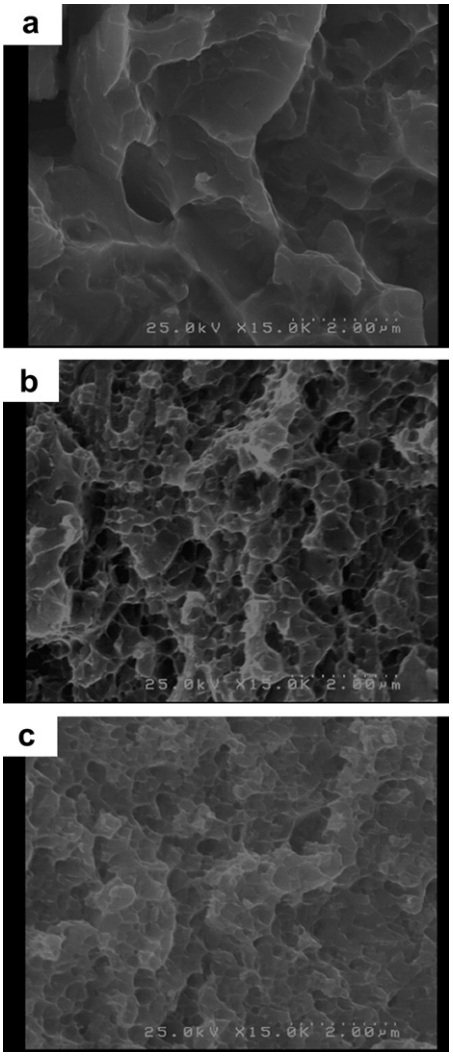

Fig. 3. SEM cross-sectional images recorded after tensile testing of the D6AC steel specimens that had been subjected to tempering at (a) RT and at (b) 250 and (c) 315 °C.

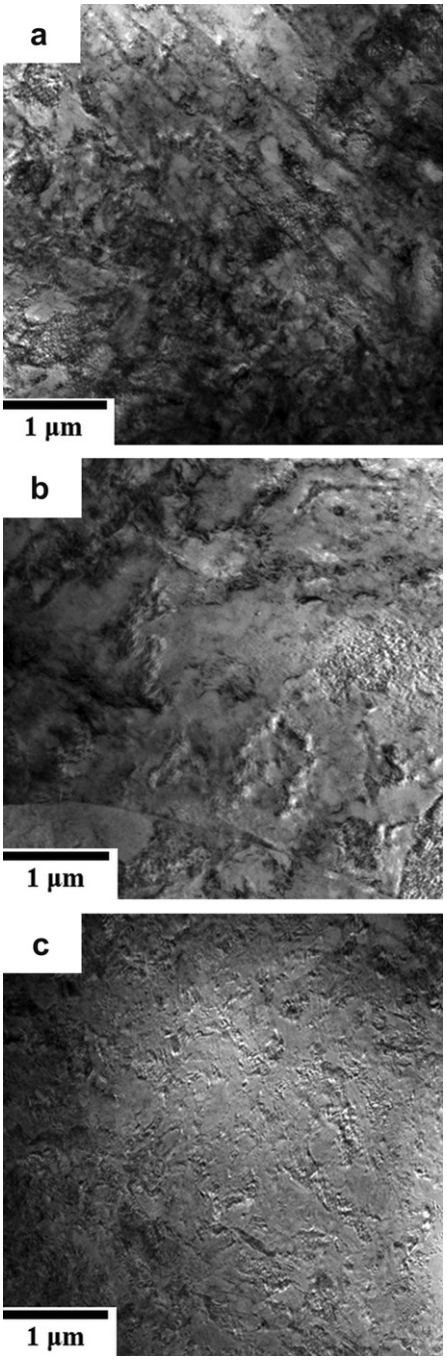

Fig. 4. Plane-view TEM image of original D6AC steel at (a) RT and at (b) 250 and (c) 315 °C.

at 250 and 315 °C, however, exhibited some intermittent values of the friction. Fig. 5(b) plots the lateral force with respect to the duration of displacement for the HAZ. In Fig. 5(c), the lateral force for the FZ was stable, with relatively minor fluctuations compared with those of the parent material and the HAZ. Fig. 6 plots typical coefficients of friction with respect to the scratch duration for all of the specimens under a ramped load of 500 μN. Pure elastic contact appeared to dominate at this low-ramped force. The friction traces were fairly reproducible, but exhibited great variability for each specimen. The plots in Fig. 4 reveal the onset of marked oscillations under the friction force and abrupt oscillations in both the on- and off-load scans. We conclude that the lower degrees of adhesion at FZ than that of HAZ due to metal bonding reflect the presence of interlinks and rearrangements. Higher degrees of adhesion at the parent material induce the causes of the fluctuations in the values of μ. We attribute this behavior to the high dislocation density contained in the weld metal; the remaining area (HAZ) was soft and ductile. The low-carbon martensitic matrix in the FZ was relatively harder than that of the parent metal (see Fig. 2). Although tempering treatment partially offset [5] the hardening effect of the samples resulting from the flow forming process, we believe that the combination of work hardening and tempering contributed considerably to the hardening effect. We suspect that the parent material was affected by the diffusion of the input fusion heat, such that part of the parent metal experienced recovery and stress relief.

It was recognized that the results of these mechanical properties of D6AC steel would be satisfied to the AMS6431M specification. In addition, we determined the effects of cold reduction, EBW, and tempering treatment on the microstructures and mechanical properties of the specimens. We found that the microstructures were dependent on the tempering treatment variables [20–24]. Finally, we performed these mechanical properties under each experimental condition, and determined the nanotribological characteristics from the HAZ and the FZ. The D6AC steel employed in this study had been subjected to a reduction in wall thickness of 67% through flow forming; we analyzed it and a blank through morphological observations.

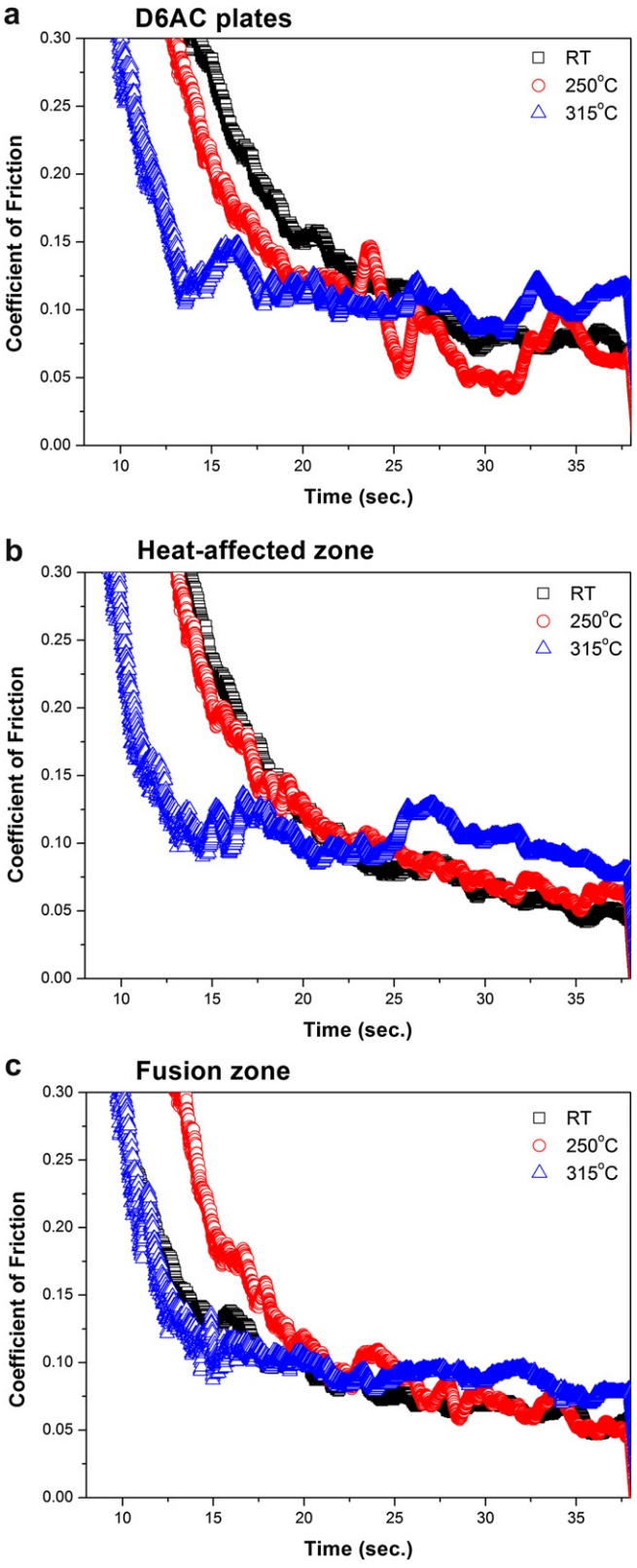

Fig. 5. Plots of lateral forces versus scratch duration for the as-deposited parent material, the HAZ, and the FZ of the D6AC steel specimens that had been subjected to tempering at (a) RT and at (b) 250 and (c) 315 °C.

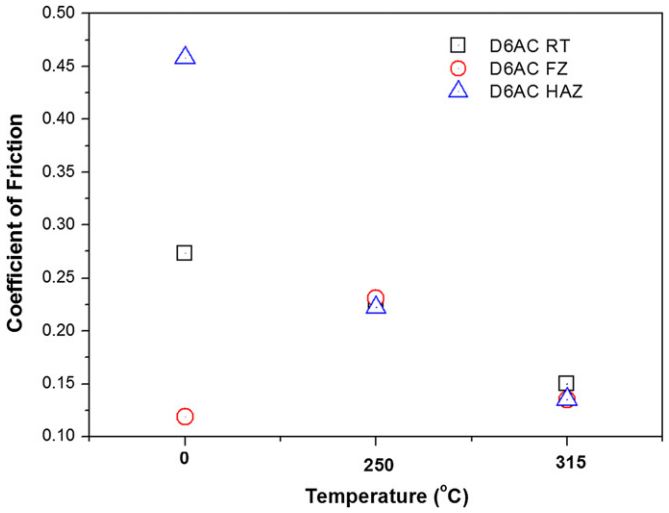

Fig. 6. Coefficients of friction of the as-deposited parent material, the HAZ, and the FZ of the D6AC steel specimens that had been subjected to tempering at RT and at 250 and 315 °C.

4. Conclusion

We have employed nanoscratch techniques to investigate the deformation of D6AC steel tubing that had been subjected to a reduction in wall thickness of 67% through flow forming and EB welding. Morphological analysis revealed that ductile rupture occurred of tempering specimens after tensile testing. In addition, the weld metal exhibited greater YS, UTS, and elongation after tempering treatment. TEM results reveal that heavily misfit dislocations by work hardening at RT and few dislocation multiplication of the samples after tempered.

Acknowledgment

The authors thank Prof. Wen-Kuang Hsu for technical support (Department of Materials Science and Engineering, National Tsing Hua University, Hsinchu, 30013, Taiwan, ROC). This study was supported by the National Science Council of the Republic of China (NSC-99-2221-E-009-031-MY2) and by the National Nano Device Laboratories in Taiwan (NDL99-C03S-042).

References

[1] Meitzner CF, Stout RD. Weld. J. 1996;45:393S–400S.
[2] Kearns WH, Semmel JW, Marble JD. Weld. J. 1960;39:484S–92S.
[3] Tsay LW, Chung CS, Chen C. Int. J. Fatigue 1997;19:25–31.
[4] Kalpakcioglu S, Rlagopal S. J. Appl. Met. Working 1982;2:211–23.
[5] Chou CP, Tsai PC, Kuo IC. Welding engineering. 1st ed. Taipei, Taiwan: Chuan Hwa Technology Publishing Company; 1991.
[6] Ashida K, Morita N, Shosida Y. JSME Int. J. Ser. C 2001;44:244–53.
[7] Lee YJ, Lee IK, Wu SC, Kung MC, Chou CP. Sci. Technol. Weld. Join. 2007;12:266–73.
[8] Lee YJ, Kung MC, Lee IK, Chou CP. Mater. Sci. Eng. A 2007;454–455:602–7.
[9] Lee YJ, Wu SC, Chang JL, Chou CP, Lee IK. Sci. Technol. Weld. Join. 2008;13:462–6.
[10] Lee IK, Chou CP, Cheng CM, Kuo IC. Mater. Sci. Technol. 2003;19:1595–602.
[11] Sivamani RK, Goodman J, Gitis NV, Maibach HI. Skin Res. Technol. 2003;9:227–34.
[12] Peterman GL. Met. Prog. 1965;87(2):80–3.
[13] Lee IK, Chou CP, Cheng CM, Kuo IC. Sci. Technol. Weld. Join. 2003;8:221–7.
[14] Quach WM, Teng JG, Chung KF. Eng. Struct. 2010;32:3501–15.
[15] Quach WM, Teng JG, Chung KF. J. Constr. Steel Res. 2009;65:1803–15.
[16] Chang TL, Tsay LW, Chen C. Mater. Sci. Eng. A 2001;316:153–60.
[17] Metals handbook. In: Magnesium alloys. 9th ed., vol. 4. Metals Park, OH: ASM International; 1981. p. 122.
[18] Bannister AC, Ruiz Ocejo J, Gutierrez-Solana F. Eng. Fract. Mech. 2000;67:547–62.

[19] Taylor JC. Düsseldorf: Pub Niobium Products Company GmbH; October 1997.
[20] Keshri AK, Bakshi SR, Chen Y, Laha T, Li X, Levy C, et al. Surf. Eng. 2009;25: 270–5.
[21] Beake BD, Bell GA, Goodes SR, Pickford NJ, Smith JF. Surf. Eng. 2010;26: 37–49.
[22] Balasubramanian TS, Balakrishnan M, Balasubramanian V, Muthu Manickam MA. Sci. Technol. Weld. Join. 2010;16:702–8.
[23] Yao ZK, Wang T, Guo HZ, Yang X. Mater. Sci. Technol. 2011;27:1701–6.
[24] Han WT, Wan FR, Leng B, Ukai S, Tang QX, Hayashi S, et al. Sci. Technol. Weld. Join. 2010;16:690–6.